Nanoscale

PAPER

View Article Online
View Journal | View Issue

Cite this: *Nanoscale*, 2024, **16**, 11310

Metal oxide hybridization enhances room temperature phosphorescence of carbon dots–SiO_2 matrix for information encryption and anti-counterfeiting†

Qing Yao, [a] Zeyu Wang,*[b] Nikolai V. Gaponenko,[c] Jindou Shi, [a] Zheyuan Da,[a] Chen Zhang,[a] Junnan Wang[a] and Minqiang Wang[a]

Room temperature phosphorescent (RTP) carbon dot (CD) materials have been widely used in various fields, but it is difficult to achieve a long lifetime, high stability and easy synthesis. In particular, realizing the phosphorescence emission of CDs using a metal oxide (MO) matrix is a challenge. Here, solid gels are synthesized *via in situ* hydrolysis, and then RTP CDs are synthesized based on a SiO_2 matrix (CDs@SiO_2) and hybridized with a MO matrix (CDs@SiO_2-MO) by high-temperature calcination. Among the materials synthesized, Al_2O_3 matrix RTP CDs (CDs@SiO_2-Al_2O_3) have a long phosphorescence lifetime of 689 ms and can exhibit yellow-green light visible to the naked eye for 9 s after the UV light (365 nm) is turned off. Compared with the green phosphorescence of CDs@SiO_2, the yellow-green phosphorescence lifetime of CDs@SiO_2-Al_2O_3 is enhanced by 420 ms. In addition, CDs@SiO_2-Al_2O_3 maintains good stability of phosphorescence emission in water, strongly oxidizing solutions and organic solvents. As a result, CDs@SiO_2-Al_2O_3 can be applied to the field of information encryption and security anti-counterfeiting, and this work provides a new, easy and efficient synthesis method for MO as an RTP CD matrix.

Received 29th March 2024,
Accepted 16th May 2024

DOI: 10.1039/d4nr01380h

rsc.li/nanoscale

1. Introduction

RTP materials have the property of emitting light for a sustained period of time after the excitation light source is turned off. After the absorption of ultraviolet and visible light, the singlet ground state (S_0) transitions to the excited state (S_1), then to the excited triplet state (T_1) through the intersystem crossing (ISC) process, and back to the ground state (S_0) to emit phosphorescence through radiative transitions.[1] Because the energy of the triplet state (T_1) is lower than that of the singlet state (S_1), there is a red-shift of the phosphorescence emission compared to the fluorescence emission. Besides, due to their unique luminescence properties, RTP materials have huge application potential in chemical sensing,[2] photocatalysis,[3] optoelectronic devices,[4,5] information encryption,[6,7] anti-counterfeiting[8–10] and bio-imaging,[11] attracting a lot of attention from many researchers. At present, the main RTP materials include rare earth phosphors,[12] organometallic complexes[13] and pure organic complexes,[14] but these traditional RTP materials have the disadvantages of a complicated preparation process, heavy metal toxicity and high cost,[15] which seriously hinder their wide application.

CDs are an emerging carbon nano-optical material with excellent biocompatibility, low cytotoxicity, a simple preparation process, easy surface functionalization and excellent optical properties,[16] so they have been widely used in bio-imaging,[17] chemical sensing[18] and opto-electronic devices.[19,20] At present, there are two main strategies to realize the phosphorescence emission of CDs;[21] one is the self-protection method: it is often adopted to enhance the phosphorescence emission of CDs by doping atoms such as B, N, and F into the CDs to improve the efficiency of the ISC from the singlet to the triplet state.[22–24] The second is the matrix-assisted method: the RTP of the CDs is generated or enhanced by embedding the CDs into various matrices, such as CDs@BA,[25] CDs@PVA,[26] CDs@SiO_2,[27] CDs@LDHs,[28] CDs@zeolite[29] and so on. Notably, the RTP CDs based on a MO matrix are novel and rarely reported. Zhang *et al.*[30] synthesized CDs@Al_2O_3 RTP materials by high-temperature pyrolysis of aluminum-

[a]*Electronic Materials Research Laboratory, Key Laboratory of the Ministry of Education International Center for Dielectric Research & Shannxi Engineering Research Center of Advanced Energy Materials and Devices, Xi'an Jiaotong University, 710049 Xi'an, China*
[b]*Frontier Institute of Science and Technology (FIST) and Micro- and Nano-technology Research Center of State Key Laboratory for Manufacturing Systems Engineering, Xi'an Jiaotong University, 710049 Xi'an, China. E-mail: zeyu.wang@xjtu.edu.cn*
[c]*Belarusian State University of Informatics and Radioelectronics, P. Browki 6, 220013 Minsk, Belarus*

†Electronic supplementary information (ESI) available. See DOI: https://doi.org/10.1039/d4nr01380h

based MOF precursors, utilizing the conversion of organic ligands in MOFs into CDs. The rigid network, strong spatial constraints and stable covalent bonding of Al_2O_3 impose multiple constraints on CDs, realizing the phosphorescence emission of CDs in Al_2O_3 matrix, which has been successfully applied in advanced dynamic information encryption and multilayer coding patterns. The phosphorescence performance of CDs@Al_2O_3 in this research work is excellent, but the synthesis process of the precursor of aluminum-based MOFs is very complicated, which leads to great difficulties in the wide application of CDs@Al_2O_3. In addition, in our previous work,[31] CDs embedded in a mesoporous magnesium oxide matrix with phosphorescence emission were realized by high-temperature pyrolysis of citric acid and $Mg_2(OH)_2CO_3$, and were successfully applied in the fields of anti-counterfeiting and photocatalysis. Although the synthesis process of CDs in mesoporous magnesium oxide in that work is facile and efficient, the phosphorescence lifetime is suboptimal. Besides, the requirement of metal-based precursor selection is stringent and not universal for other metal oxides (*e.g.*, Zn, Al, *etc.*). Generally speaking, it is difficult to achieve phosphorescence emission from CDs in a MO matrix because the synthesis of MO often requires high temperatures (400–700 °C), which is a great challenge for conventional carbon source precursors. Therefore, choosing a suitable precursor to protect the CDs from carbonization at high temperatures and forming an effective covalent bond with the MO to achieve phosphorescence emission is the major emphasis in the synthesis of CDs@MO RTP materials.

In this work, ammonium citrate and metal chloride added to tetraethyl orthosilicate (TEOS) were stirred at room temperature for 4 h in the presence of ammonia to form a solid gel. After that, RTP CD materials were synthesized by high temperature calcination. Compared with CDs@SiO_2, after the UV light (365 nm) was turned off, the duration of RTP of CDs@SiO_2-MO was significantly improved and the phosphorescence color changed from green to yellow-green. The phosphorescence performance of CDs@SiO_2-Al_2O_3 was the most outstanding, with the phosphorescence lifetime reaching 689 ms, and the yellow-green RTP lasted more than 9 s and was visible to the naked eye. In addition, CDs@SiO_2-Al_2O_3 can emit phosphorescence in water, strongly oxidizing agents and various organic solvents and shows good stability. Therefore, CDs@SiO_2-Al_2O_3 can be further applied in the fields of phosphorescence anti-counterfeiting and information encryption, which significantly improves the security of information identification and encryption.

2. Results and discussion

Briefly, CDs@SiO_2 was synthesized by stirring ammonium citrate with TEOS in the presence of ammonia for 4 h at room temperature and centrifuging for 10 minutes at 9000 rpm until a solid gel was formed, followed by calcination at a high temperature (Fig. 1). For the synthesis of CDs@SiO_2-MO, metal chloride was added to the precursor solution, and the subsequent synthesis was carried out in the same way as for CDs@SiO_2 (see details in the Experimental section in the ESI†). The synthesized CDs@SiO_2 was only able to exhibit green phosphorescence visible to the naked eye for less than 2 s after the UV light (365 nm) was turned off. However, it is exciting to note that the phosphorescence color of the synthesized CDs@SiO_2-MO changes from green to yellow-green and the duration of RTP visible to the naked eye is greatly improved by hybridizing with the MO matrix. Among the materials studied, CDs@SiO_2-Al_2O_3 shows the best performance, with the RTP lasting more than 9 s (Fig. 2d), which is at a high level among the RTP CD materials.

Transmission electron microscopy (TEM) images in Fig. 2a and b show the morphology of CDs@SiO_2; it can be observed that the CDs are dispersed in the SiO_2 matrix, and the XRD pattern of CDs@SiO_2 shows the presence of a silica phase (Fig. S1†). In addition, it can be seen in the high-resolution

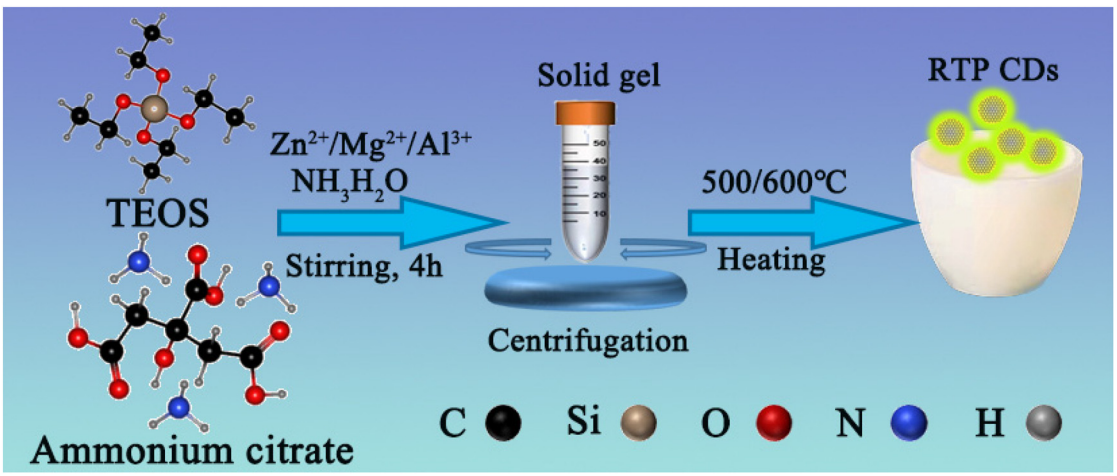

Fig. 1 Schematic illustration of the synthesis of CDs@SiO_2 and CDs@SiO_2-MO.

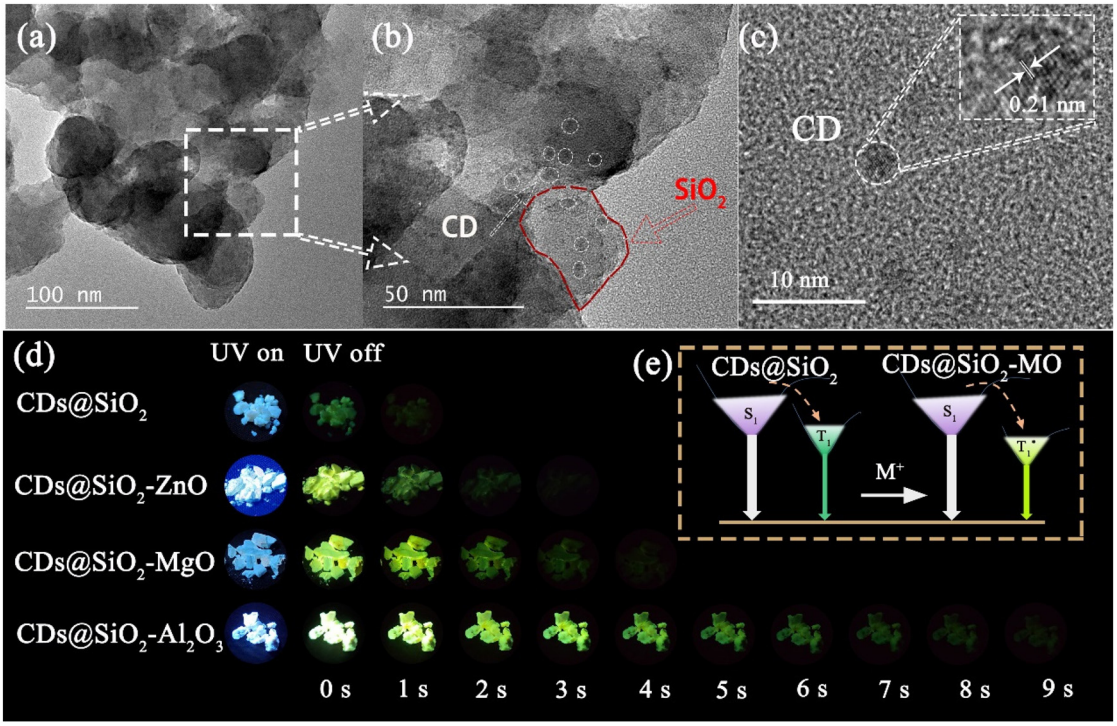

Fig. 2 (a–c) TEM and HRTEM images of CDs@SiO_2. (d) Photographs of the CDs@SiO_2 and CDs@SiO_2-MO powder excited with a 365 nm UV lamp and after turning off UV. (e) Possible fluorescence and phosphorescence emission processes of CDs@SiO_2 and CDs@SiO_2-MO.

TEM (HRTEM) image (Fig. 2c) that the CDs are embedded in the SiO_2 matrix with a size of about 4 nm and the lattice stripe spacing is 0.21 nm.[32] For CDs@SiO_2-MO, Fig. S2a and S3a† show the TEM images of CDs@SiO_2-MgO and CDs@SiO_2-ZnO, respectively. Moreover, the TEM images of CDs@SiO_2-Al_2O_3 are shown in Fig. S4 and S5a.† It can be observed that CDs@SiO_2-ZnO is round shaped with a size of about 500 nm, and the morphology of CDs@SiO_2-MgO and CDs@SiO_2-Al_2O_3 is an irregular flake morphology, which may be due to the fact that the growth of ZnO has very little effect on the morphology of SiO_2. Fig. S2, S3 and S5† show the scanning electron microscopy (SEM) energy dispersive spectrometry (EDS) mapping of CDs@SiO_2-ZnO, CDs@SiO_2-MgO and CDs@SiO_2-Al_2O_3, respectively, showing the uniform presence of the elements C, O, Si, and Zn/Mg/Al. The above results are in agreement with the X-ray diffraction (XRD) pattern analysis (Fig. S1†), which proves that CDs@SiO_2-ZnO, CDs@SiO_2-MgO and CDs@SiO_2-Al_2O_3 are composed of CDs, SiO_2 and the corresponding metal oxides, respectively.

X-ray photoelectron spectroscopy (XPS) and Fourier transform infrared spectroscopy (FT-IR) were performed to further determine the functional groups and the chemical composition of samples. The XPS spectrum shows that CDs@SiO_2 contains three elements: Si, C and O (Fig. 3a). Fig. 3b shows that the high-resolution C1s spectrum deconvoluted to two peaks at 284.7 eV and 285.5 eV, which are attributed to C–C/C═C and C–O, respectively.[33] The high-resolution O1s spectrum (Fig. 3c) contains two peaks at 533.1 eV and 533.9 eV corresponding to Si–O/C–O and O–H. For CDs@SiO_2-Al_2O_3, the XPS spectrum (Fig. 3d) shows four elements: Si, C, O, and Al, and the atomic concentrations of Si, C, O, and Al are 21.47%, 12.2%, 58.12%, and 8.21%, respectively. The element N is almost undetectable in the CDs@SiO_2-Al_2O_3 product because the amino groups are oxidized to the gas of nitrogen oxides during pyrolysis. As shown in Fig. 3e, the high-resolution C1s spectrum deconvoluted to three peaks at 284.7 eV, 285.6 eV and 287.1 eV, which are attributed to C–C/C═C, C–O and C═N,[34] respectively. The XPS spectrum of O1s (Fig. 3f) exhibits two peaks at binding energies of 532.6 eV (Al–O) and 533.1 eV (C–O).[35] Compared to CDs@SiO_2, the high-resolution C1s deconvolution spectrum of CDs@SiO_2-Al_2O_3 shows the presence of C═N bonds. This is due to the fact that the addition of $AlCl_3$ to the precursor allows for more retention of the N element (generation of NH_4Cl), and thus the difference in the N content of the samples affects the type of functional group on the surface of the CDs, which leads to the difference in optical properties between CDs@SiO_2 and CDs@SiO_2-Al_2O_3. Similarly, the XPS spectra of CDs@SiO_2-ZnO and CDs@SiO_2-MgO were also investigated as shown in Fig. S6.† The presence of the C═N bond is also seen in the high-resolution deconvolution spectrum of the C1s, which further demonstrates that the existence of differences in optical properties between CDs@SiO_2-MO and CDs@SiO_2 is closely related to the type of functional group on the surface of the CDs. The FT-IR spectra of CDs@SiO_2, CDs@SiO_2-ZnO, CDs@SiO_2-MgO and CDs@SiO_2-Al_2O_3 are shown in Fig. 4a, with O–H stretching vibrations at 3490 cm^{-1}, Si–H stretching vibrations at 2090 cm^{-1}, anti-symmetric stretching vibrations of Si–O–Si at

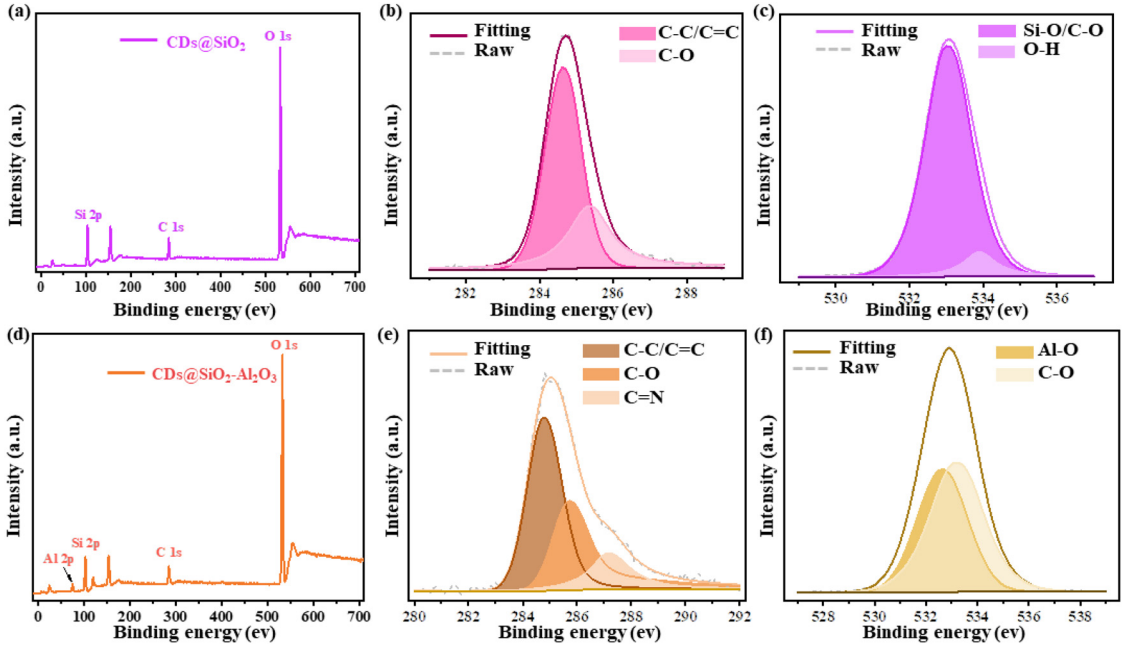

Fig. 3 (a) XPS spectra of CDs@SiO_2 and (b and c) high-resolution XPS spectra of C 1s and O 1s. (d) XPS spectra of CDs@SiO_2-Al_2O_3 and (e and f) high-resolution XPS spectra of C 1s and O 1s.

1055 cm^{-1} and Si–C stretching vibrations at 800 cm^{-1}.[36–38] It can be observed that the order of Si–O–Si and Si–C stretching vibrational strengths is CDs@SiO_2 > CDs@SiO_2-ZnO > CDs@SiO_2-MgO > CDs@SiO_2-Al_2O_3, which may be due to the fact that the CDs in CDs@SiO_2-Al_2O_3 are better embedded into the Al_2O_3 matrix, and the rigid network of the porous structure combines with the CDs more tightly, leading to the weakening of the surface functional group vibration. It also reflects that the CDs embedded in an Al_2O_3 matrix produce a greater covalent bond binding strength, which generates more stable triplet states and suppresses the non-radiative transition, leading to a longer RTP lasting time (consistent with the actual results in Fig. 2d).

The UV-Vis absorption spectra in Fig. 4b show that wide-peak absorption exists at 220–350 nm for CDs@SiO_2 and CDs@SiO_2-MO, in which the optimal absorption peaks are located at 267 nm for CDs@SiO_2 and at 320 nm for CDs@SiO_2-MO, corresponding to the π–π* and n–π* transitions in the conjugated structure,[39,40] respectively. This indicates that the green phosphorescence emission of CDs@SiO_2 excited with a UV source is mainly associated with the π–π* transition of CDs, and the yellow-green phosphorescence emission of CDs@SiO_2-MO is mainly related to the n–π* transition. The difference in the UV absorption spectra between CDs@SiO_2 and CDs@SiO_2-MO is mainly due to the difference in the N element content of the CDs, resulting in differences in the surface functional groups or edge defects.[41] The maximum values of fluorescence and RTP emission wavelengths of CDs@SiO_2 are 370 and 480 nm, corresponding to the excitation wavelength of 270 nm, as shown in Fig. 4f. A significant excitation dependence of the fluorescence and phosphorescence emission of CDs@SiO_2 can be seen in Fig. 4d and e, where the fluorescence emission wavelength is red-shifted from 350 nm to 460 nm and the phosphorescence emission wavelength is red-shifted from 470 nm to 520 nm as the excitation wavelength is increased from 260 nm to 400 nm. However, for CDs@SiO_2-Al_2O_3, the optimal fluorescence and RTP emission wavelengths were 387 nm and 520 nm, corresponding to an excitation wavelength of 320 nm, as shown in Fig. 4i. When the excitation wavelength was increased from 310 nm to 400 nm, the fluorescence emission wavelength was red-shifted from 380 nm to 485 nm and the phosphorescence emission wavelength was red-shifted from 470 nm to 575 nm, as shown in Fig. 4g and h. Besides, the fluorescence and phosphorescence emission spectra of CDs@SiO_2-ZnO and CDs@SiO_2-MgO were investigated and they also exhibited similar luminescence properties to CDs@SiO_2-Al_2O_3, as shown in Fig. S7.†

The CIE coordinates (Fig. 5a) of CDs@SiO_2 and CDs@SiO_2-Al_2O_3 are (0.22, 0.39) and (0.31, 0.014), respectively, indicating that CDs@SiO_2 and CDs@SiO_2-Al_2O_3 emit green and yellow-green RTP. The afterglow decay spectra (Fig. 4c) of CDs@SiO_2, CDs@SiO_2-ZnO, CDs@SiO_2-MgO and CDs@SiO_2-Al_2O_3 were also tested, and their average lifetimes were calculated to be 269 ms, 367 ms, 379 ms and 689 ms, respectively, according to the equation $\tau_{avg} = \frac{\sum \alpha_i \tau_i^2}{\sum \alpha_i \tau_i}$. It can be seen that CDs@SiO_2-MO shows a great improvement in phosphorescence lifetime and RTP lasting time compared to CDs@SiO_2. In particular, the phosphorescence lifetime of CDs@SiO_2-Al_2O_3 is increased by 420 ms and the lasting time of RTP visible to the naked eye is enhanced by 8 s compared to that of CDs@SiO_2. According to

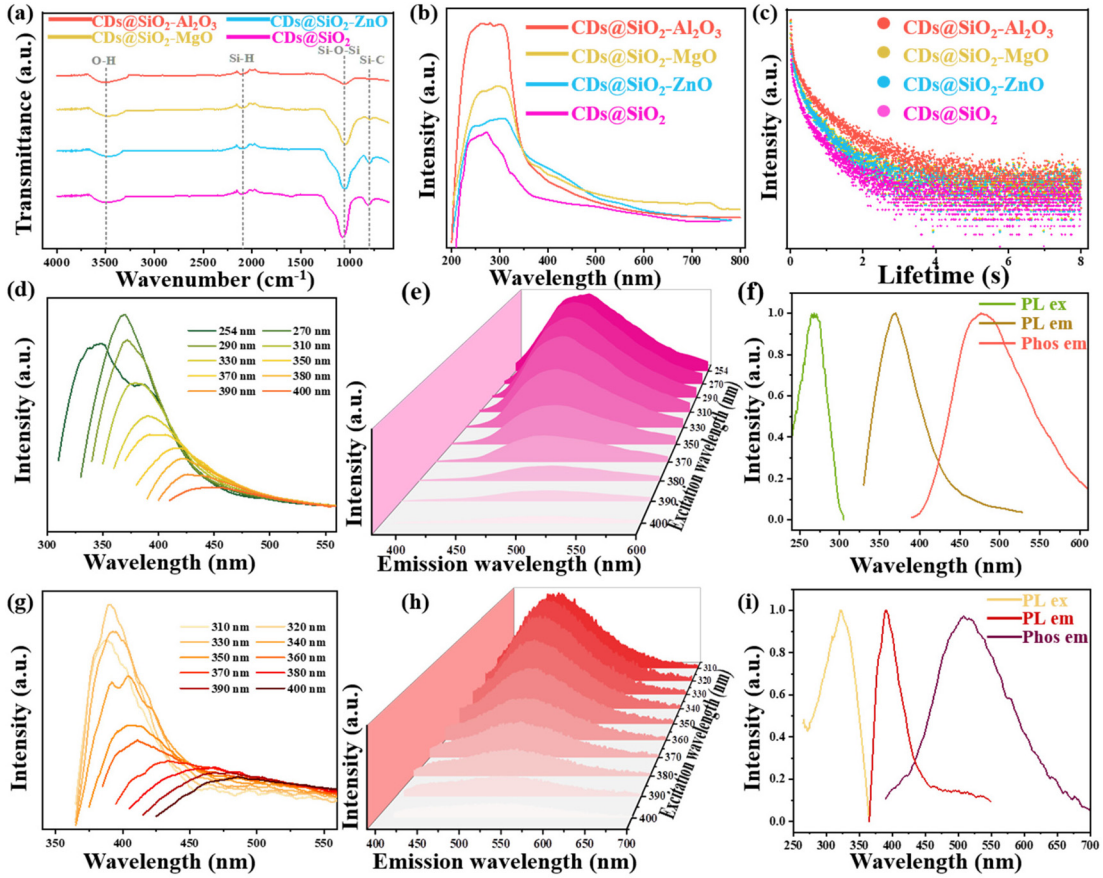

Fig. 4 (a) FT-IR patterns of CDs@SiO_2 and CDs@SiO_2-MO. (b) UV-Vis absorption spectra of CDs@SiO_2 and CDs@SiO_2-MO. (c) Phosphorescence decay curves of CDs@SiO_2 and CDs@SiO_2-MO. (d and e) Fluorescence and phosphorescence emission spectra of CDs@SiO_2 at different excitation wavelengths. (f) Optimal excitation, fluorescence and phosphorescence emission spectra of CDs@SiO_2. (g and h) Fluorescence and phosphorescence emission spectra of CDs@SiO_2-Al_2O_3 at different excitation wavelengths. (i) Optimal excitation, fluorescence and phosphorescence emission spectra of CDs@SiO_2-Al_2O_3.

previous research work,[42,43] the RTP properties of CDs@SiO_2-Al_2O_3 are given and compared with those of other similar RTP CD complexes in Table S1.† In addition, the temperature-dependent phosphorescence emission spectra were also observed, as shown in Fig. 5b. At 77 K, the CDs@SiO_2-Al_2O_3 powder showed the strongest emission at 525 nm, and the peak intensity gradually decreased with increasing temperature, resulting from an effective restriction of vibrational motion and suppression of nonradiative transitions at low temperatures, which indicates its remarkable phosphorescence properties.[44] Similarly, a maximum phosphorescence lifetime of 1120 ms at 77 K was tested, significantly higher than the 689 ms at 300 K, as shown in Fig. 5c. Considering the requirement of material stability in practical applications, we evaluated the anti-burst performance and stability of CDs@SiO_2-Al_2O_3. As demonstrated in Fig. S8,† the as-prepared CDs@SiO_2-Al_2O_3 samples were put into water and strongly oxidizing agents (H_2O_2 and H_2SO_4) and left to stabilize for 30 min. Surprisingly, the fluorescence and phosphorescence of CDs@SiO_2-Al_2O_3 showed good stability, and RTP could be observed for as long as that of the solid powder. In addition, CDs@SiO_2-Al_2O_3 was dispersed in different polar solvents, including DMF, cyclohexane and methanol. Similarly, CDs@SiO_2-Al_2O_3 exhibited the same excellent stability and RTP lasting time in organic polar solvents.

Since the RTP properties of CDs@SiO_2 and CDs@SiO_2-Al_2O_3 were enabled during high-temperature calcination, we further investigated the mechanism of their RTP (Fig. 2e and Fig. 6a). Typically, under the excitation of UV light, the ground state (S_0) of CDs can absorb energy to transition to the excited state (S_1), and the excited state (S_1) returns to S_0 to emit fluorescence. However, covalent bonds such as O–H, Si–O–C and Al–O–C can be generated during the calcination process to impose restrictions on the vibration of the surface functional groups of CDs, resulting in the transfer of energy from S_1 to T_1 (the ISC process) to create phosphorescence emission.[45,46] The T_1 state energy of CDs@SiO_2 is higher than that of CDs@SiO_2-Al_2O_3 due to the different types of surface functional groups and the covalent bond binding strengths of CDs with the matrix. Thus, after removing the excitation UV source (365 nm), CDs@SiO_2 emits green phosphorescence while CDs@SiO_2-Al_2O_3 emits yellow-green phosphorescence with a

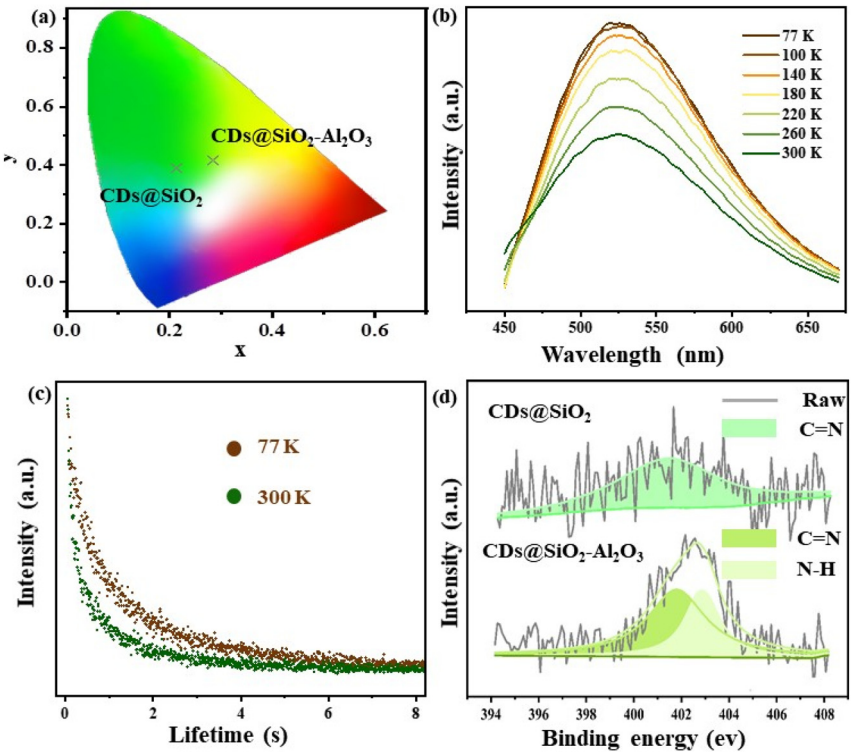

Fig. 5 (a) CIE coordinates of $CDs@SiO_2$ and $CDs@SiO_2$-Al_2O_3. (b) Variable-temperature phosphorescence spectra of $CDs@SiO_2$-Al_2O_3. (c) Phosphorescence decay curves of $CDs@SiO_2$-Al_2O_3 at 77 k and 300 k. (d) High-resolution XPS spectra of N 1s for $CDs@SiO_2$ and $CDs@SiO_2$-Al_2O_3.

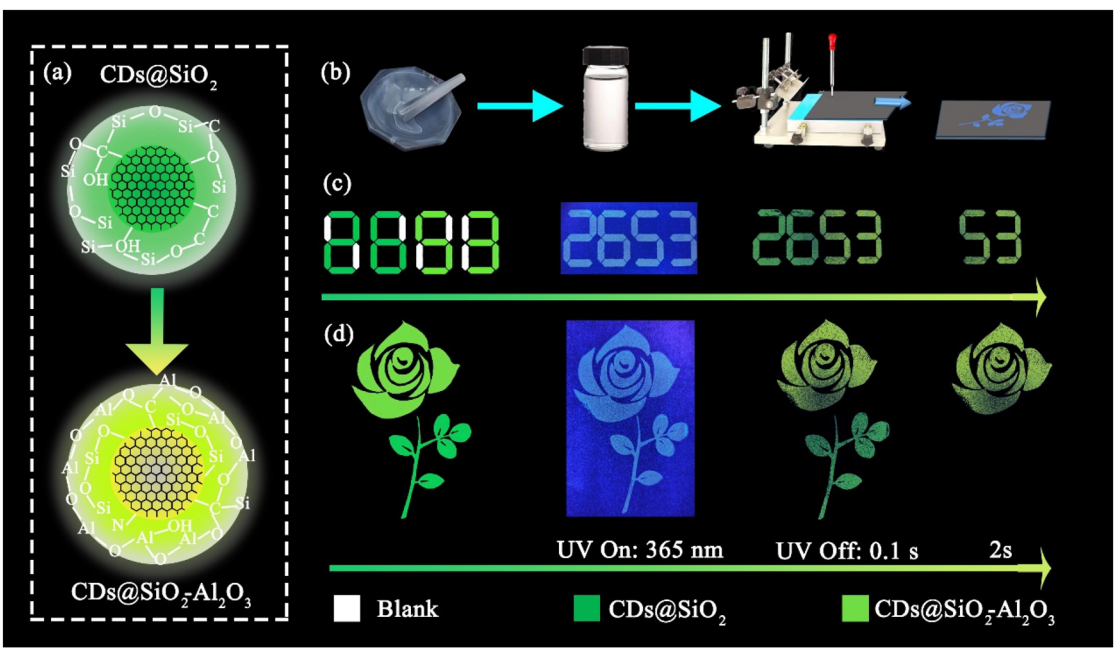

Fig. 6 (a) Schematic illustration of the phosphorescence emission mechanism of $CDs@SiO_2$ and $CDs@SiO_2$-Al_2O_3. (b) Screen printing flowchart of anti-counterfeiting patterns. (c and d) Information encryption and anti-counterfeiting applications of digital and floral patterns.

40 nm redshift, as shown in Fig. S9.† Furthermore, the phosphorescence lifetime of $CDs@SiO_2$-Al_2O_3 is much longer than that of $CDs@SiO_2$, which is an attractive phenomenon. It is considered that there are two main reasons; the first one is due to the addition of $AlCl_3$ to the precursor during the synthesis of $CDs@SiO_2$-Al_2O_3, which produces NH_4Cl leading to

more N sources being retained after high-temperature calcination. Thus, CDs@SiO_2-Al_2O_3 has a higher content of functional C═N bonds on the surface of the CDs than CDs@SiO_2 (Fig. 5d), and the N atoms in the carbon lattice can adequately disorientate the electron network, which is homogeneously conjugated. This network regulates the surface properties by adjusting the charge distribution and spinning culture of doped domains.[47] The above analysis concludes that the presence of more N atoms in the carbon lattice changes the surface functional group properties or causes more defects, resulting in a longer phosphorescence lifetime of CDs@SiO_2-Al_2O_3. The second reason is that a porous Al_2O_3 matrix is synthesized during the high temperature calcination process. The CDs are excellently embedded into the Al_2O_3 framework network and are more tightly bonded to the Al_2O_3 framework network compared to other matrices. From the FT-IR analysis shown in Fig. 4e, it can be seen that the vibrational intensity of the functional groups on the surface of CDs@SiO_2-Al_2O_3 is the lowest, which indicates that the covalent bonding network of CDs@SiO_2-Al_2O_3 has a higher binding strength, making the triplet state of the CDs more stable and it better inhibits the non-radiative transition, leading to a longer phosphorescence lifetime.

Since CDs@SiO_2 and CDs@SiO_2-Al_2O_3 have different phosphorescence emission wavelengths and varied phosphorescence lifetimes, they can be applied in advanced anti-counterfeiting and information encryption. In Fig. 6b, the screen printing process flow of the anti-counterfeiting pattern is shown, in which the RTP CD powder is first fully ground in a mortar and then mixed with an appropriate amount of glue, and the anti-counterfeiting printed pattern is obtained on a printing table by using the scraping and coating method. Fig. 6c shows that when irradiated with a 365 nm UV lamp, the blue luminescent number "2653" is visible because both emit blue fluorescence. After turning off the UV lamp for 0.1 s, the green luminescent digit "26" is visible along with the yellow-green luminescent digit "53". Because of the long phosphorescence lifetime of CDs@SiO_2-Al_2O_3, after turning off the UV lamp for 2 s, the green phosphorescence of CDs@SiO_2 disappeared and only the yellow-green luminescent digit "53" was visible. Similarly, as shown in Fig. 6d, when the pattern was irradiated with a 365 nm UV lamp, both the leaves and the flower emitted blue light. After turning off the light for 0.1 s, green leaves and a yellow-green flower were visible. However, only the yellow-green flower pattern could be seen after turning off the light for 2 s. The above results indicate that the as-prepared RTP CDs have good application value in information encryption and anti-counterfeiting.

3. Conclusions

In summary, we utilized the hydrolysis and condensation reaction of TEOS in the presence of ammonia to generate a solid gel, adding ammonium citrate and metal chloride to the precursor to obtain CDs@SiO_2-MO by high temperature calcination. Among the materials studied, CDs@SiO_2-Al_2O_3 showed a long phosphorescence lifetime of 689 ms and the RTP visible to the naked eye lasted more than 9 s. Compared with CDs@SiO_2, CDs@SiO_2-MO possesses more N atoms in the carbon lattice which change the surface functional group properties, resulting in a phosphorescence emission color variation from green to yellow-green after the 365 nm UV lamp is turned off. In addition, the porous Al_2O_3 matrix framework binds more tightly to the CDs, resulting in stronger covalent bonding to the surface groups of the CDs, causing more stable triplet state emission for a longer phosphorescence lifetime. Owing to the excellent phosphorescence properties of CDs@SiO_2-Al_2O_3, it can be successfully applied to the field of information encryption and anti-counterfeiting. Furthermore, this work provides a new idea for efficient and simple synthesis of RTP CDs with a MO matrix.

Author contributions

Qing Yao: conceptualization (lead), investigation (lead), methodology (lead), and writing – original draft preparation (lead); Zeyu Wang: conceptualization (equal), funding acquisition (lead), and writing – review and editing (lead); Nikolai V. Gaponenko: investigation (equal); Jindou Shi: investigation (equal); Zheyuan Da: investigation (equal); Chen Zhang: investigation (equal); Junnan Wang: conceptualization (equal); and Minqiang Wang: investigation (equal).

Conflicts of interest

There are no conflicts to declare.

Acknowledgements

This work was supported by the National Basic Research Program of China (973 Program) (2022YFE0122500 and 2019YFB1503200), the National Natural Science Foundation of China (NSFC, 52161145103 and 61774124), the 111 Program (No. B14040), and the Shanxi Provincial Key Research and Development Project (No. 2021GXLH-Z-084).

References

1 X. Wei, J. Yang, L. Hu, Y. Cao, J. Lai, F. Cao, J. Gu and X. Cao, *J. Mater. Chem. C*, 2021, **9**, 4425–4443.
2 C. Wang, Y. Chen, Y. Xu, G. Ran, Y. He and Q. Song, *ACS Appl. Mater. Interfaces*, 2020, **12**, 10791–10800.
3 X. Fang, Y. Tang, Y.-J. Ma, G. Xiao, P. Li and D. Yan, *Sci. China Mater.*, 2023, **66**, 664–671.
4 B. Zhou, Z. Qi, M. Dai, C. Xing and D. Yan, *Angew. Chem., Int. Ed.*, 2023, **62**, e202309913.
5 C. Xing, B. Zhou, D. Yan and W.-H. Fang, *Adv. Sci.*, 2024, **11**, 2310262.

6 Y.-C. Liang, K.-K. Liu, X.-Y. Wu, Q. Lou, L.-Z. Sui, L. Dong, K.-J. Yuan and C.-X. Shan, *Adv. Sci.*, 2021, **8**, 2003433.
7 C. Xing, Z. Qi, B. Zhou, D. Yan and W.-H. Fang, *Angew. Chem., Int. Ed.*, 2024, e202402634.
8 Y. Sun, S. Liu, L. Sun, S. Wu, G. Hu, X. Pang, A. T. Smith, C. Hu, S. Zeng, W. Wang, Y. Liu and M. Zheng, *Nat. Commun.*, 2020, **11**, 5591.
9 C. Xing, B. Zhou, D. Yan and W.-H. Fang, *CCS Chem.*, 2023, **5**, 2866–2876.
10 G. Xiao, Y.-J. Ma, Z. Qi, X. Fang, T. Chen and D. Yan, *Chem. Sci.*, 2024, **15**, 3625–3632.
11 Y.-C. Liang, S.-S. Gou, K.-K. Liu, W.-J. Wu, C.-Z. Guo, S.-Y. Lu, J.-H. Zang, X.-Y. Wu, Q. Lou, L. Dong, Y.-F. Gao and C.-X. Shan, *Nano Today*, 2020, **34**, 100900.
12 Z. Chen, K. Y. Zhang, X. Tong, Y. Liu, C. Hu, S. Liu, Q. Yu, Q. Zhao and W. Huang, *Adv. Funct. Mater.*, 2016, **26**, 4386–4396.
13 X.-Y. Dong, Y. Si, J.-S. Yang, C. Zhang, Z. Han, P. Luo, Z.-Y. Wang, S.-Q. Zang and T. C. W. Mak, *Nat. Commun.*, 2020, **11**, 3678.
14 O. Bolton, K. Lee, H.-J. Kim, K. Y. Lin and J. Kim, *Nat. Chem.*, 2011, **3**, 205–210.
15 J. Jia, W. Lu, Y. Gao, L. Li, C. Dong and S. Shuang, *Talanta*, 2021, **231**, 122350.
16 A. Ghaffarkhah, E. Hosseini, M. Kamkar, A. A. Sehat, S. Dordanihaghighi, A. Allahbakhsh, C. van der Kuur and M. Arjmand, *Small*, 2022, **18**, 2102683.
17 Q. Zhang, R. Wang, B. Feng, X. Zhong and K. Ostrikov, *Nat. Commun.*, 2021, **12**, 6856.
18 Y. Ma, A. Y. Chen, Y. Y. Huang, X. He, X. F. Xie, B. He, J. H. Yang and X. Y. Wang, *Carbon*, 2020, **162**, 234–244.
19 H. Choi, S.-J. Ko, Y. Choi, P. Joo, T. Kim, B. R. Lee, J.-W. Jung, H. J. Choi, M. Cha, J.-R. Jeong, I.-W. Hwang, M. H. Song, B.-S. Kim and J. Y. Kim, *Nat. Photonics*, 2013, **7**, 732–738.
20 B. Zhao, Z. Wang and Z. a. Tan, *Nat. Photonics*, 2020, **14**, 130–131.
21 F. Gu and X. Ma, *Chem. – Eur. J.*, 2022, **28**, e202104131.
22 P. Long, Y. Feng, C. Cao, Y. Li, J. Han, S. Li, C. Peng, Z. Li and W. Feng, *Adv. Funct. Mater.*, 2018, **28**, 1800791.
23 B. Zhao, R. Yu, K. Xu, C. Zou, H. Ma, S. Qu and Z. a. Tan, *J. Mater. Chem. C*, 2021, **9**, 15577–15582.
24 F. Liu, Z. Li, Y. Li, Y. Feng and W. Feng, *Carbon*, 2021, **181**, 9–15.
25 W. Li, W. Zhou, Z. Zhou, H. Zhang, X. Zhang, J. Zhuang, Y. Liu, B. Lei and C. Hu, *Angew. Chem., Int. Ed.*, 2019, **58**, 7278–7283.
26 Y. Deng, D. Zhao, X. Chen, F. Wang, H. Song and D. Shen, *Chem. Commun.*, 2013, **49**, 5751–5753.
27 W. Li, S. Wu, X. Xu, J. Zhuang, H. Zhang, X. Zhang, C. Hu, B. Lei, C. F. Kaminski and Y. Liu, *Chem. Mater.*, 2019, **31**, 9887–9894.
28 R. Wang, Y. Zhu, Z. Xia, K. Liang, L. Kong, J. Liu, W. Shi and C. Lu, *J. Mater. Chem. C*, 2022, **10**, 17182–17189.
29 J. Liu, N. Wang, Y. Yu, Y. Yan, H. Zhang, J. Li and J. Yu, *Sci. Adv.*, 2017, **3**, e1603171.
30 L. Zhang, X. Chen and Y. Hu, *Small*, 2024, **20**, 2305185.
31 Q. Yao, H. Wu, J. Liang, C. Wang, Y. Jin, Y. Hu and Y. Tang, *Sci. China Mater.*, 2024, **67**, 170–178.
32 J. Chen, J. Tan, P. Liang, C. Wu, Z. Hou, K. Shen, B. Lei, C. Hu, X. Zhang, J. Zhuang, L. Sun, Y. Liu and M. Zheng, *Small*, 2024, **20**, 2306323.
33 J. Li, X. Zhao and X. Gong, *Adv. Opt. Mater.*, 2024, **12**, 2302297.
34 Y. Xian and K. Li, *Adv. Mater.*, 2022, **34**, 2201031.
35 H. Liu, N. u. H. Tariq, Y. Ren, X. Li, X. Cui, J. Wang and T. Xiong, *Appl. Surf. Sci.*, 2022, **601**, 154234.
36 T. H. Kim, A. R. White, J. P. Sirdaarta, W. Ji, I. E. Cock, J. St John, S. E. Boyd, C. L. Brown and Q. Li, *ACS Appl. Mater. Interfaces*, 2016, **8**, 33102–33111.
37 E. S. Park, H. W. Ro, C. V. Nguyen, R. L. Jaffe and D. Y. Yoon, *Chem. Mater.*, 2008, **20**, 1548–1554.
38 F. Wang, Z. Xie, H. Zhang, C.-y. Liu and Y.-g. Zhang, *Adv. Funct. Mater.*, 2011, **21**, 1027–1031.
39 L. Tang, R. Ji, X. Cao, J. Lin, H. Jiang, X. Li, K. S. Teng, C. M. Luk, S. Zeng, J. Hao and S. P. Lau, *ACS Nano*, 2012, **6**, 5102–5110.
40 W. Li, S. Wu, H. Zhang, X. Zhang, J. Zhuang, C. Hu, Y. Liu, B. Lei, L. Ma and X. Wang, *Adv. Funct. Mater.*, 2018, **28**, 1804004.
41 L.-L. Li, J. Ji, R. Fei, C.-Z. Wang, Q. Lu, J.-R. Zhang, L.-P. Jiang and J.-J. Zhu, *Adv. Funct. Mater.*, 2012, **22**, 2971–2979.
42 R. Gao, M. S. Kodaimati and D. Yan, *Chem. Soc. Rev.*, 2021, **50**, 5564–5589.
43 Q. Huang, Z. Lin and D. Yan, *Small Struct.*, 2021, **2**, 2100044.
44 K. Wan, Y. Zhai, S. Liu, J. Li, S. Li, B. Strehmel, Z. Chen and T. D. James, *Angew. Chem., Int. Ed.*, 2022, **61**, e202202760.
45 J. Liu, Y. Luo, Z. Ran, F. Wang, M. Sun, Y. Luo, J. Zhuang, X. Zhang, B. Lei, Y. Liu and C. Hu, *Chem. Eng. J.*, 2023, **474**, 145597.
46 Y. Liu, X. Kang, Y. Xu, Y. Li, S. Wang, C. Wang, W. Hu, R. Wang and J. Liu, *ACS Appl. Mater. Interfaces*, 2022, **14**, 22363–22371.
47 X.-K. Kong, C.-L. Chen and Q.-W. Chen, *Chem. Soc. Rev.*, 2014, **43**, 2841–2857.